Water Air Soil Pollut (2014) 225:1987
DOI 10.1007/s11270-014-1987-9

Removal of Humic Acid by Organo-Montmorillonites: Influence of Surfactant Loading and Chain Length of Alkylammonium Cations

M. Fernández · G. Curutchet · R. M. Torres Sánchez

Received: 30 January 2014 / Accepted: 28 April 2014
© Springer International Publishing Switzerland 2014

Abstract In this study, the characterization and adsorption properties of montmorillonite (MMT) and organomontmorillonites with different surfactant/cationic exchange capacity (CEC) ratios (1 and 2) of tetradecyl trimethylammonium ($TDTMA^+$) and hexadecyl trimethylammonium ($HDTMA^+$) cations were evaluated. The particle apparent diameter, determined by laser and scanning electron microscopy showed aggregate formation, which varied with loading and cation length of the surfactant used. X-ray diffraction analysis revealed the formation of a pseudotrilayer arrangement of both surfactants in the interlayer space, FTIR showed the characteristic bands of the surfactants and micelle formations, and zeta potential determinations indicated neutral or negative surface charge values, except for sample obtained with one CEC concentration exchanged with $HDTMA^+$ (HDTMA1-MMT) where a charge reversal to positive was found. Higher adsorption amounts of humic acid (HA) were found for HDTMA1-MMT and TDTMA1-MMT samples than for MMT sample, while the increase in the loading of both surfactants decreased the amounts of HA adsorbed could be assigned to a higher micelle formation and different packing density of alkyl chain, in the external surface. The correlation found between the total surface area and negative zeta potential values and the HA adsorption rate, within each surfactant, indicated the strong influence that these properties have on HA adsorption.

Keywords Humic acid · Organo-montmorillonites · Adsorption · $HDTMA^+$ surfactants · $TDTMA^+$ surfactants

1 Introduction

Soluble humic substances (mainly humic and fulvic acids) are organic molecules found as natural components of soils that are potentially important ligands for various polyvalent metal ions with significant effects on their transport in aquatic systems (Furukawa and Takahashi 2008). The presence of soluble humic substances in water, generally are not considered as an organic pollutant, while the modifications produced in water quality as turbidity, taste, etc. need to be modified to attain a safe water use. Particularly, the presence of humic acids in water serve as substrate for bacterial growth, bind with heavy metals and pesticides to yield high concentrations of these substances, enhancing their transportation in water (Doulia et al. 2009), and react with chlorine used for water treatment leading to the evolution of chlorinated organic compounds, some of them known as human carcinogens (trihalomethanes, White 1999).

Electronic supplementary material The online version of this article (doi:10.1007/s11270-014-1987-9) contains supplementary material, which is available to authorized users.

M. Fernández · R. M. Torres Sánchez (✉)
CETMIC-CCT La Plata,
Camino Centenario y 506, (1897) M. B. Gonnet, La Plata, Argentina
e-mail: rosats@cetmic.unlp.edu.ar

G. Curutchet
Laboratorio de Análisis Ambiental, Instituto de Investigación e Ingeniería Ambiental, Universidad Nacional de San Martín, Buenos Aires, Argentina

Published online: 17 May 2014

Clay minerals, particularly montmorillonite (MMT) and kaolinite, are important inorganic soil components involved in the sorption of a large variety of inorganic and organic contaminants. Water sediments, within which clays participate (Dekov et al. 1997), are main depositories of organic debris, where both organic matter and humic acids are involved.

In both systems, the knowledge of clay/humic acid interaction is critical to understand the behavior of these natural systems.

The use of MMT as an adsorbent is related mainly to its low cost, high cation exchange capacity, and large internal and external surfaces. It was largely utilized to adsorb heavy metals, antibiotics, several environmental pollutants, water remediation, eliminate water turbidity, etc. (Jiang et al. 2004; Avisar et al. 2010; Klepsch et al. 2011; Fernández et al. 2011; Goldani et al. 2013).

Modification of clay surfaces, in order to create new sorption capacity, can be obtained by thermal or mechanical treatment, ion exchange reactions, etc., and therefore allows its use in innovative applications (nanocomposite precursors, removal of organic pollutants, development of environmentally oriented pesticide formulations, treatment of waste effluents, etc. (Theng et al. 2008; Froehner et al. 2009; Ruiz-Hitzky et al. 2010).

Particularly, organomontmorillonite (OMMT), obtained from MMT by replacement of the raw inorganic interlayer cations by organic cations through ion exchange reactions, were first reported in 1939 (Gieseking 1939). The clay surface changes from highly hydrophilic to hydrophobic, and besides, new sorption sites, positive electric charge (Bianchi et al. 2013), and increase of the interlayer space of MMT result from the different loading of long-chain alkylammonium cations (He et al. 2010). The hydrophobic characteristics of OMMT samples enhance their adsorption, with respect to raw clays, and allow them to remove anionic and nonpolar organic contaminants from water (Park et al. 2011). Particularly, the quaternary amines with long alkyl chains strongly bind to sorbents in the aquatic environment such as suspended sediment and humic acid (HA), due to their multiple sorptive interactions. This behavior postulated the organoclays as promising adsorbents of a wide variety of organic molecules (Anirudhan and Ramachandran 2007 and references therein). It is usually assumed that carbon chains sorb the organic fraction of both suspended sediment and humic acid through van der Waals forces.

Humic acids from different origins can also be removed by such positively charged OMMT because they contain multiple negative charges. The sorption mechanisms of OMMT from water are influenced by the structure of the exchanged organic moiety. If the organic moiety is a long-chain surfactant, partition of the humic acids to the organic phase created by the adsorbed surfactants was considered to be the predominant mechanism (Anirudhan and Ramachandran 2007; Zhan et al. 2010). An added value is the fact that amines with alkyl chains between C14 and C16 adsorbed on montmorillonite decreased its toxicity (Wijk et al. 2009) and allows them to be used in water treatment.

In this paper, attention was focused on the effect of the loading (one and two times the cation exchange capacity) and alkyl chain length (tetradecyl- and hexadecyl–trimethyl–ammonium bromide) of OMMT on HA adsorption at neutral pH. The physical and electric surface charge properties and morphology changes of OMMT were studied by measurements of specific surface area, particle size determination, zeta potential measurements, and scanning electron microscopy (SEM). The interlayer changes generated by the surfactant loading in MMT and those in surface properties were analyzed by x-ray diffraction (XRD). Also, Fourier transform infrared spectroscopy (FTIR) and zeta potential measurements were utilized to characterize the OMMT-HA complex formed.

2 Experimental

2.1 Materials

An Argentinean smectite, provided by Castiglioni Pes y Cia., was used as raw material. This sample was characterized previously (Magnoli et al. 2008) and its main properties are mineral content: 84, 4, and 12 % of montmorillonite, quartz, and feldspars, respectively; cation exchange capacity (CEC) 174 meq/100 g, isoelectric point (IEP_{pH}=2.7), external surface area (determined by N_2 adsorption) 34.0 m^2/g, and total specific surface area (determined by water vapor adsorption, Michot and Villieras 2006 621 m^2/g. The chemical analysis, determined on a sample of purified MMT, indicated the structural formula $[(Si_{3.89}\ Al_{0.11})\ (Al_{1.43}\ Fe_{0.26}\ Mg_{0.30})]\ M^{+}_{0.41}$, which allows its classification as a highly charged smectite (0.41 eq./formula unit) (Magnoli et al. 2008).

The hexadecyl–trimethyl–ammonium ($HDTMA^+$) and the tetradecyl–trimethyl–ammonium ($TDTMA^+$) bromides were purchased from Aldrich Chemical Company Inc. and used as received (98 and 99 % purity, respectively) with 50 and low milligram per milliliter solubility in water and molecular weight of 364.5 and 336.41 g mol^{-1}, respectively.

Humic acid was purchased from Aldrich and was further purified according to the procedure of Vermeer et al. (1998).

2.2 Methods

2.2.1 Organo–Montmorillonite Preparation

The OMMTs were obtained by the following procedure: a determined amount of the cationic surfactants was dissolved in 200 mL, and 6 g of MMT was added and stirred for 5 h at 60 °C. The concentrations of $HDTMA^+$ and $TDTMA^+$ bromides used were one and two times the CEC of MMT, respectively. All products were washed by centrifugation to free them of bromide anions (tested by $AgNO_3$), dried at 80 °C, and ground in an agate mortar. The OMMT samples were denoted indicating the alkyl ammonium cations and their loading respect to the CEC concentration (i.e., HDTMA1-MMT, TDTMA2-MMT, etc.). HDTMA1-MMT and HDTMA2-MMT samples were characterized in previous work (Bianchi et al. 2013) by XRD diffraction, specific surface area, apparent diameter, and zeta potential curve determinations.

2.2.2 Surface, Particle Size, and Morphology Characterization

The external specific surface area (ESSA) was determined by N_2 adsorption (BET method, at −196 °C) using a Quantachrome Autosorb instrument and the total surface area (TSA), by water vapor adsorption at a relative humidity (RH) of 0.56 as described elsewhere (Torres Sánchez and Falasca 1997). For OMMT, sites for water adsorption were not specifically determined as in raw clays, so even though the same methodology was used, this parameter does not indicate their specific surface.

Particle size determination was performed by dynamic light scattering (DLS) measurements using a Brookhaven 90Plus/Bi-MAS Multi Angle Particle Sizing Instrument, operating at λ=635 nm, 15-mW solid state laser, scattering angle of 90 ° and temperature of 25 °C. Particles were dispersed in water solutions to attain 0.05 % *w/w* suspensions and sonicated for 10 min. The determination only gives an apparent equivalent sphere diameter (Dapp).

The morphology of the MMT and OMMT samples was examine by scanning electron microscopy (SEM) using a field emission gun scanning electron microscope Zeiss (FEG-SEM Zeiss LEO 982 GEMINI). MMT and OMMT samples were fixed to 10-mm metal mounts using carbon tape, and spit coated with gold under vacuum in an argon atmosphere.

2.2.3 Adsorption of HA by OMMT

The adsorption experiments were carried out by adding 1 mL of the MMT or OMMT sample suspensions (1 % *w/w*) to 9 mL of HA solutions in a concentration range up to 300-mg humic acid/L. Before conducting the adsorption experiments, preliminary kinetic studies were carried out (Fernández 2012) and 12 h was found to be long enough to reach equilibrium in agreeing with that indicated by Anirudhan and Ramachandran (2007) for HA adsorption on HDTMA-MMT loading with 100 % the CEC at pH 3. The pH of the dispersions was 7. After 24-h contact time, with continuous stirring, the suspensions were centrifuged for 20 min at 14,000 rpm and the supernatants collected and analyzed by UV spectrophotometry (maximum absorption λ= 254 nm) using a Hewlett-Packard 8453 UV-visible spectrophotometer. The amount of HA adsorbed was determined as the difference between initial concentration and that of the supernatant in equilibrium. The adsorption experiments were made at least by duplicate. Samples with maximum HA adsorbed were washed twice by centrifugation for 20 min at 14,000 rpm, and the supernatants were collected, dried at 80 °C overnight, and kept in a desiccator for further studies.

2.2.4 FTIR Measurements

KBr-pressed discs of dried samples were analyzed by FTIR in a PerkinElmer Inc. (spectrum one model) instrument in the spectral range 4,000–400 cm^{-1}, in air at room temperature.

2.2.5 XRD Determinations

A Philips 3020 apparatus was used to record x-ray diffraction (XRD) patterns (001 reflection), in the range

of $3 \leq 2\theta \leq 13$ °. The operating conditions were: 40 kV and 30 mA, Cu Kα radiation, Ni filter, a step width of 0.02 °, and 2.0 s/step counting time. Samples were oriented at constant humidity (dispersion samples were dried maintaining a constant RH of 0.47 for 48 h).

2.2.6 Surface Charge Measurements

The zeta potential was determined by microelectrophoresis in the same Brookhaven equipment (Zeta potential function) utilized for Dapp measurement, using 10^{-3} M KCl as inert electrolyte and Pd electrodes. Sample suspensions (0.5 g L^{-1}) were equilibrated at several pH values by adding HCl or KOH.

3 Results and Discussion

3.1 Adsorbent Characterization

The total surface area (TSA), external specific surface area (ESSA) and apparent particle diameter (Dapp) of all samples are indicated in Fig. 1.

The ESSA value for MMT, as was indicated previously (Magnoli et al. 2008), agrees with values indicated elsewhere (Bojemueller et al. 2001). The decrease in ESSA values up to 94 %, with the exchange of both alkylammonium salts, was also previously observed and assigned to the diminution of micropore size, and surfactant occupancy of the interparticle pores in the OMMT samples (Praus et al. 2006; Bianchi et al. 2013; Park et al. 2011).

The decrease of TSA values was directly related to the alkylammonium salt concentration that caused a hydrophobic environment for OMMT samples. The strong interactions generated by the alkylammonium salt arrangement in the MMT interlayer (Pospíšil et al. 2002), and in the external surfaces (determined by zeta potential measurements, Zadaka et al. 2010) impede water vapor adsorption and determine the TSA drop up to more than 90 % (TSA value for HDTMA2-MMT=19 m^2/g) respect to the value for MMT sample (573 m^2/g).

The rise in OMMT aggregate values (Fig. 1), indicated by Dapp measurements, with respect to that obtained for MMT, as will be further explained by the zeta potential curve analysis, was associated with the alkylammonium salt loading and also with surfactant micelle formation (Radian et al. 2011) in the external OMMT surfaces. The influence of alkylammonium salt loading on MMT was previously studied for HDTMA loading between 0.4 and 4.0 times the CEC (Naranjo et al. 2013) and different adsorption mechanism of the surfactant on the MMT surface were concluded. For surfactant loading higher than 1 times the CEC, as those studied in this work, a weak adsorption mechanism is proposed, where interactions of the carbon tails of the surfactant molecules in solution and molecules adsorbed in the interlayer occurs, generating higher aggregates than those obtained for low surfactant loading. In order to clarify the capability of micelle formation, it is important to indicate that to achieve the values of 1 and 2 times the CEC, there was an excess used of 14 and 27 times for $TDTMA^+$ and 56 and 116 times for $HDTMA^+$ of the critical micelle concentration values, (CMC=3.8 and 0.9 mM for $TDTMA^+$ and $HDTMA^+$, respectively, Fuguet et al. 2005). The micelle interaction with the surface left many positive head groups exposed to the solution and consequently, electrostatic attraction participated to increase the OMMT aggregate sizes measured as Dapp. Also, the different binding coefficients of the monomers adsorbed (Zadaka et al. 2010), their affinity (Mishael et al. 2002) for the clay surface and higher packing arrangements on the external surface with chain length increase (Shah et al. 2013) contribute to form the different aggregate sizes obtained.

The SEM image (Fig. 2a) revealed that the MMT sample had the typical smectite morphology (curly edges and a leaf-like structure, He et al. 2006) forming a relatively compact structure. SEM images of TDTMA1- and TMTA2-MMT samples (Fig. 2b, c were similar to SEM images of HDTMA1- and HDTMA2-MMT samples, in Bianchi et al. 2013) were considerably different from that of the MMT sample and similar to that found for HDTMA-Wyoming montmorillonite (He et al. 2006). OMMT samples (Fig. 2b, c and that for HDTMA-MMT shown in Bianchi et al. 2013) had a uniform size of about 1 μm and higher agglomeration than that obtained for MMT sample, in agreement with the Dapp data found (Fig. 1), while no differences can be determined between the different loading and alkylammonium length chains.

3.2 HA Adsorption and HA Complex Characterization

The equilibrium adsorption data were fitted to Langmuir isotherm model and maximal adsorption amounts of HA at pH 7 was obtained from the respective adsorption

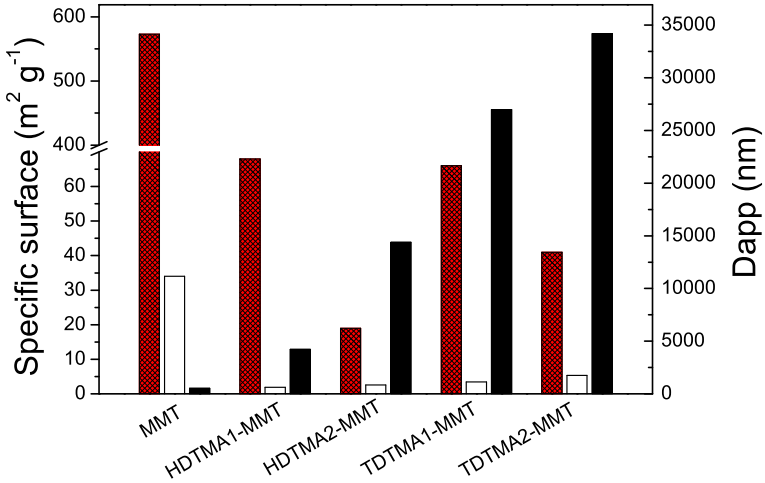


Fig. 1 Specific surface areas and apparent diameter for indicated samples. Bar symbols: *black bars* Dapp; *red spotted bars* TSA, and *white bars* ESSA

curves (figure not shown). The maximum monolayer adsorption capacity were 80 and 50 mgHA/g clay, for HDTMA1-MMT and TDTMA1-MMT samples, respectively, improving the 40 mgHA/g clay data value found for MMT sample, and those found by Anirudhan and Ramachandran (2007) on HDTMA-MMT with 100 % of CEC exchanged at pH 3.0. However, maximal adsorption amounts of HA, attained values of 50 and 30 mgHA/g clay for HDTMA2-MMT and TDTMA2-MMT samples. The HA adsorption values obtained for HDTMA1-MMT and TDTMA1-MMT samples are higher the 45 mg/g HA adsorbed, referred by Daifullah et al. (2004) by activated carbon from rice husk with a specific surface of 376 m^2/g. The decrease in adsorption amount with the increase in the loading of both surfactants indicated that electrostatic interactions play an important role in the adsorption mechanism. Those electrostatic interactions would be reduced by increase of interactions of the surfactant carbon tails in solution with the surfactant molecules adsorbed in the interlayer (Naranjo et al. 2013) with the surfactant loading increase from one to two times the CEC. In Fig. 3a, b, HA adsorption is indicated as a percentage of HA removal vs. HA added for all samples studied. In Fig. 3, the adsorption enhancement of HA, produced by OMMT adsorbents with respect to MMT

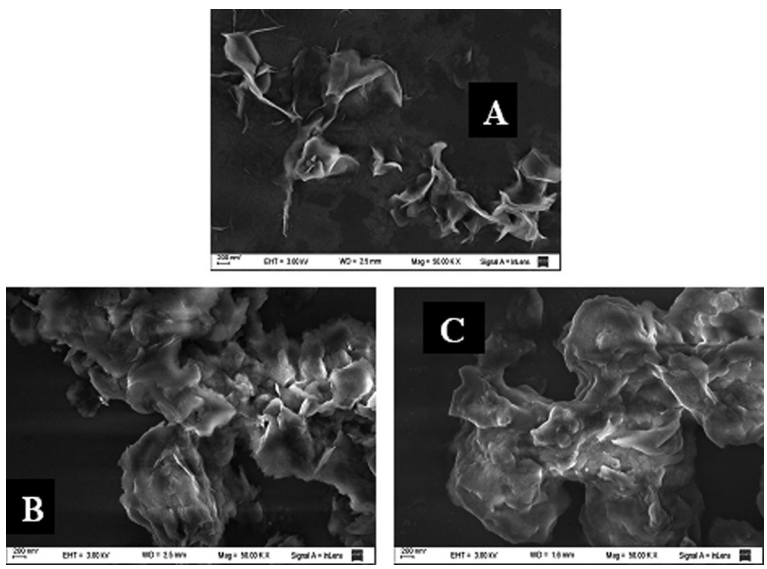


Fig. 2 SEM micrographs of **a** MMT, **b** TDTMA1-MMT, and **c** TDTMA2-MMT samples

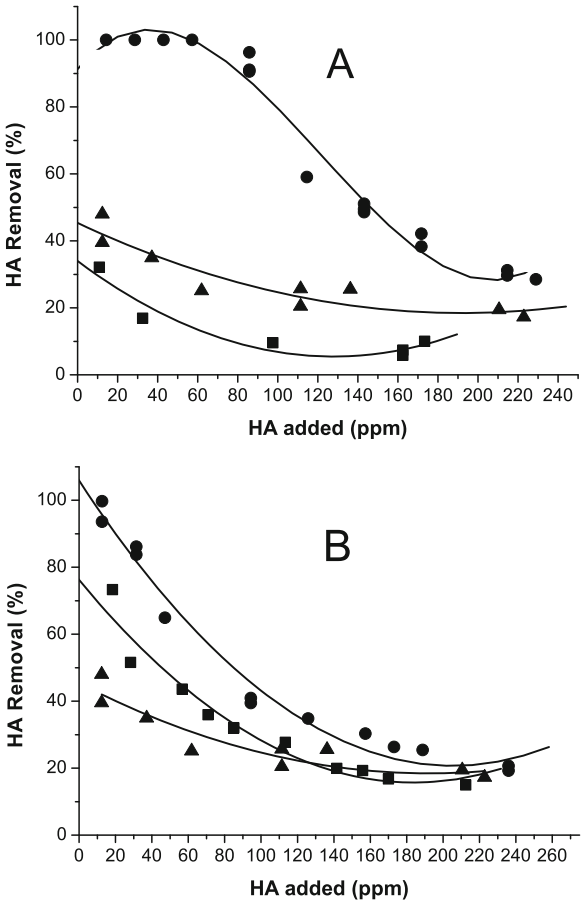


Fig. 3 HA removal by **a** $HDTMA^+$ and **b** $TDTMA^+$: *triangles* MMT, *circles* 1-CEC-MMT, and *squares* 2-CEC-MMT

sample, is important, especially at low HA concentrations (up to 20 ppm) close to those concentrations at which HA is ubiquitous in aquatic systems (Frimmel and Christman 1988).

The difference in the adsorbed amount of HA by MMT of around 40 % with that found by Radian et al. (2011), at initial HA concentration up to 20 ppm, can be assigned to the higher CEC of the MMT used in this work with respect to the CEC=74 meq/100 g indicated by these authors.

For OMMT samples, the adsorption percentage obtained in all concentration ranges studied was related to the decrease of TSA values. Which, in turn, was developed by the presence of the surfactant in each sample studied (Fig. 1). The fact whether the surface charge would also be related to the HA percentage adsorption found for both surfactants and its amount will be discussed in the following paragraphs.

3.3 XRD Analysis

The d001 value obtained from XRD patterns (Fig. 4) indicated a shift to higher basal spacing (from 1.24 to around 2.20 nm for MMT and OMMT samples, respectively) with the entrance of alkylammonium cations into the interlayer. According to the model of Lagaly and Weiss (1970), the intercalation process increases the basal spacing, depending on the length of the alkyl chains and the surface charge of the MMT. Following the arrangement models proposed for the adsorbed surfactants within the MMT interlayer spaces (lateral-monolayer, ~1.5 nm; lateral-bilayer, ~1.7 nm; pseudotrilayer, ~2.0 nm; paraffin-monolayer, ~2.4 nm; and paraffin bilayer, ~4.0 nm, (Zhu et al. 2003; Lagaly and Weiss 1970), both alkylammonium cations would be arranged as pseudotrilayer, in agreement with that reported for low-layer charge MMT samples loaded with HDTMA (He et al. 2006).

For OMMT samples, the loading increase of HDTMA or TDTMA from one to two CEC, produced a slight decrease in the respective OMMT basal space of 0.075 and 0.157 nm, respectively (Fig. 4). Taking into account the basal space of a completely anhydrous MMT of 0.97 nm (Lombardi et al. 2006), both surfactants generate an increase of interlayer space of around 1.20 or 1.10 nm for two and one CEC, respectively.

Particularly for $TDTMA^+$, Park et al. (2011) reported similar basal spacing for a low-layer charge MMT loaded with one and three times of CEC concentrations, concluding from shoulders found in the 001 reflection that there were two arrangements of $TDTMA^+$ in the

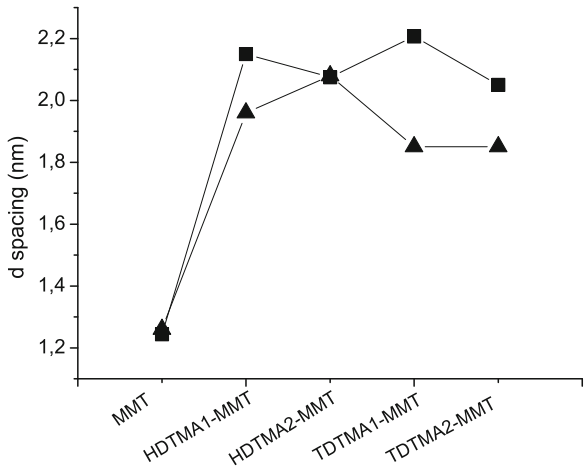


Fig. 4 Basal plane distances for indicated samples; *squares* without and *triangles* with HA

interlayer, as a lateral bilayer and as a pseudotrilayer. The absence of the lateral bilayer arrangement in our samples could be assigned to the different layer charge MMT used and to the OMMT synthesis temperature.

It is known that surfactant micelle formation is affected not only by the surfactant, but also by temperature, ionic strength, pH, etc. Noudeh et al. (2007) reported a decrease in CMC of 20 % and 32 %, for $TDTMA^+$ and $HDTMA^+$, respectively, with a temperature gap from 35 to 25 °C. Hence, the higher temperature of synthesis used in our work, despite the coincidence of alkylammonium concentrations used, could originate a high concentration of monomers in solution, which in turn, could produce the single arrangement of surfactants found in the interlayer space.

The characterization of HDTMA2-MMT sample by small angle (SAXS) and wide angle (WAXS) x-ray scattering curves (Bianchi et al. 2013) revealed the formation of a greater interlayer space, which generated the arrangement of $HDTMA^+$ as paraffin-like bilayers with a tilt angle of approximately 60 ° (Zhu et al. 2003), in addition to the pseudo three-layer arrangement mentioned above.

For MMT sample, the adsorption of HA does not change the 001 reflection as was reported previously (Li et al. 2003). Adsorption of HA on OMMT samples produced a decrease in basal spacing (Fig. 4) of 0.36 and 0.20 nm for TDTMA1-MMT and for TDTMA2-MMT and HDTMA1-MMT samples, respectively. These decreases in basal spacing found with HA adsorption could be assigned to changes of the surfactant arrangements from pseudotrilayer to lateral bilayer, where the increase of surfactant as in HDTMA2-MMT sample prevented a significant HA-surfactant interlayer interaction.

3.4 FTIR Characterization

OMMT samples studied by FTIR revealed two moderate intense bands at 3,629 and 3,425 cm^{-1} (figure not shown) that were ascribed to the stretching frequencies of the structural OH functional group. However, broad bands at around 3,400 cm^{-1} were assigned to other water hydrogen bonded to interlayer water molecules (Park et al. 2011).

The absorption bands at 2,800–3,000 cm^{-1} corresponded to the asymmetric ν_{as} (CH_2) stretching modes of the surfactant (Radian et al. 2011). Similar results (Fig. 5a) have been reported by Park et al. (2011), where it was indicated that the shift to low wavenumber of bands at 2,926 and 2,855 cm^{-1} for OMMT samples reflects the formation of a solid-like molecular environment. In addition, bands at 1,480–1,450 cm^{-1} (Fig. 5a) and those at 740–710 cm^{-1} (figure not shown) were assigned to interlayer packing density of alkyl chain assemblies (Zhu et al. 2005).

The peak at 3,030 cm^{-1} was assigned to the asymmetric stretching mode of the methyl groups attached to the positively charged amine group (Li et al. 2008). For HDTMA- and TDTMA-MMT samples (Fig. 5a) this band was found at 3,017 cm^{-1} and evidenced micelle adsorption on the MMT surface (Radian et al. 2011).

The IR analysis of HA sample showed the following absorption bands: 3,400 cm^{-1} arising from H-bonded OH groups (figure not shown), 1,620–1,600 cm^{-1} produced by aromatic C=C vibrations, 1,400 cm^{-1} due to OH deformation (Fig. 5b) and C–O stretching or C–H deformation of CH_3 groups, and 1,050 cm^{-1} assigned to C–O stretching (Stevenson and Goh 1971). These characteristic band of HA in adsorbed samples were overlapped with the large water bands at 3,400–3,620 and

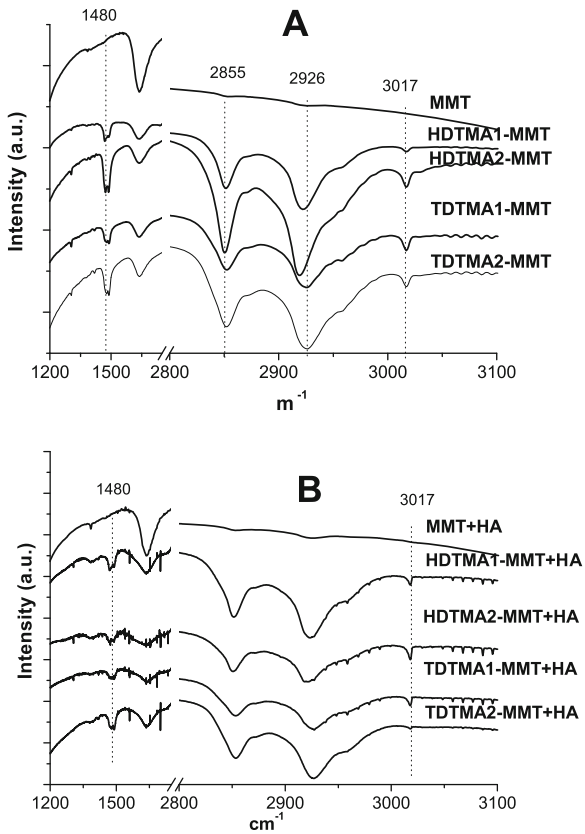


Fig. 5 FTIR spectra of indicated samples

1,550–1,750 cm^{-1} and to stretching Si–O vibration at 1,050 cm^{-1} of the MMT (Fig. 5b). While the permanence of the band at 3,017 cm^{-1} in OMMT samples indicated the persistence of micelles after HA adsorption.

3.5 Zeta Potential Measurements

The zeta potential curves from pH 3 to 10 of MMT and TDTMA-MMT samples are presented in Fig. 6a. The MMT sample showed the classical negative and flat curve indicating a pH-independent negative surface charge (Thomas et al. 1999; Lombardi et al. 2006), originated in the structure or basal sites of constant surface potential and the edge sites of variable charge.

A charge reversal, with increasing amount of $TDTMA^+$ (Fig. 6a) and $HDTMA^+$ (Bianchi et al. 2013) up to one CEC, was found; this behavior was assigned to a progressive coverage of the edge and external surface by alkylammonium groups such as micelles, and also to a higher packing arrangements on the external surface with chain length increase (Shah et al. 2013). The $HDTMA^+$ and $TDTMA^+$ loading of two CEC reduced the zeta potential values of OMMT, keeping it positive for HDTMA2-MMT sample (+20 mV at pH 3, +5 mV at pH 6 and +15 mV at pH 7, Bianchi et al. 2013), while a reversal to negative charge appeared for TDTMA2-MMT sample (−10 mV at pH 6 and −14 mV at pH 7; Fig. 6a). In a previous work (Bianchi et al. 2013), a similar behavior to the MMT loaded with octadecyl trimethyl ammonium one and two times the concentration of the CEC was found, which developed a lower decrease in zeta potential positive regard to the same loading with HDTMA. These zeta potential behaviors with both surfactant loading was also assigned to the packing arrangements of alkyl chain assemblies (Zhu et al. 2005) and also to the interaction that produced higher aggregates (Naranjo et al. 2013). In fact, a direct shift of the decrease of the zeta potential values with the excess of each surfactants, respect to the respective CMC values, was found (deposited as supplementary material), which indicate that the amount of micelle present in each OMMT samples are related to the zeta potential values obtained.

The zeta potential differences between both OMMT samples could be caused by the competition of two different arrangements of the adsorbed surfactants as a function of their loading amount and the respective CMC value. These behaviors were indicated by Praus et al. (2006) and Radian et al. (2011) as being bilayer arrangements with some positive ammonium groups oriented out of the surface and micelle formation, where not all ammonium groups interacted with the surface and were exposed to the solution.

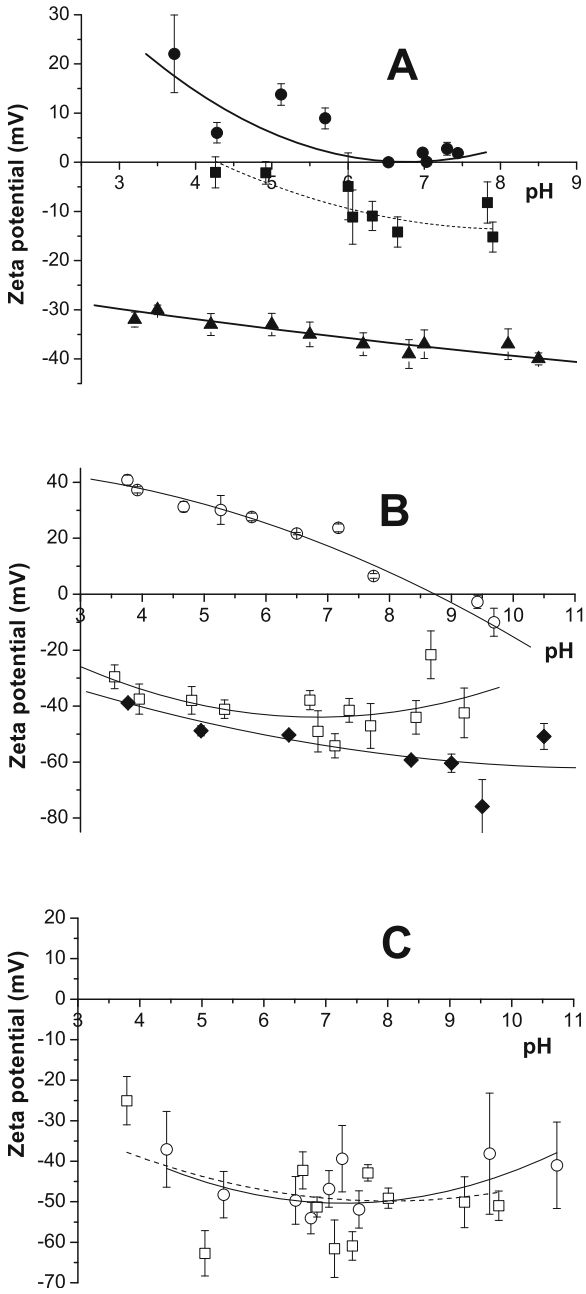


Fig. 6 Zeta potential as a function of pH for: **a** *triangles* MMT and *circles* TDTMA1-MMT and *squares* TDTMA2-MMT samples; **b** *open circles* HDTMA1-MMT-HA, *open squares* HDTMA2-MMT-HA and *diamonds* HA; **c** *open circles* TDTMA1-MMT-HA and *open squares* TDTMA2-MMT-HA

Figure 7 indicates the relationship between the HA percentage adsorbed (at C_o=20 and 140 ppm) and the zeta potential values which indicated the electric surface charge status of MMT sample and OMMT samples with the respective surfactant loading increase (HDTMA and TDTMA, respectively). As can be seen in Fig. 7, HDTMA and TDTMA, for all samples, the HA percentage adsorbed was closely related to the zeta potential, decreasing with the increase of HA added. However, for each surfactant the HA adsorption percentage was inversely correlated with the surfactant amount loaded (lower HA percentage adsorbed for higher surfactant loading). Different degrees of micelle surface formation between both surfactants (indicated by the excess of each surfactants, in respect to the respective CMC values) which originated different surface arrangements

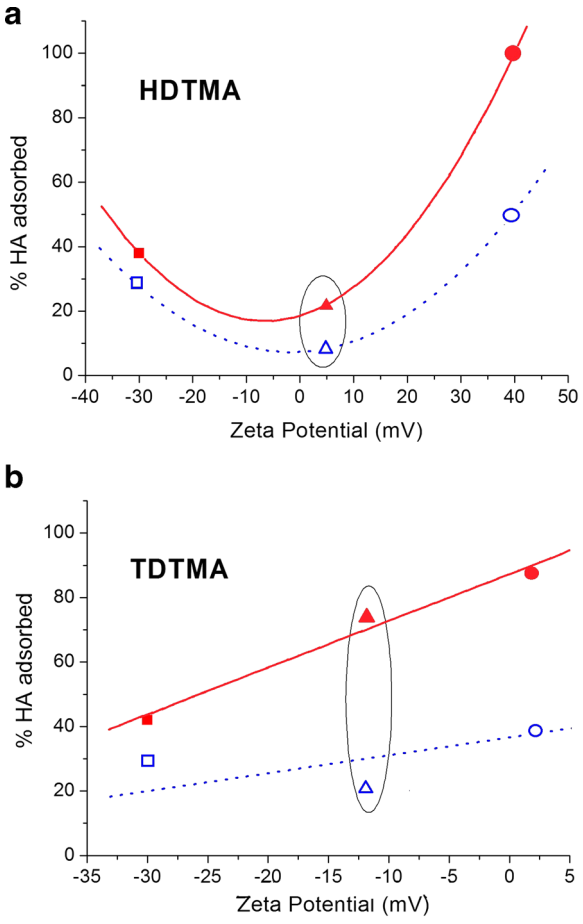


Fig. 7 Relationship of HA percentage adsorbed (C_o = *full red line* 20 and *dotted blue line* 140 ppm) with the Zeta potential (at pH 7), for *squares* MMT and OMMT samples with surfactants (HDTMA and TDTMA) loading c*ircles* one and *triangles* two times the CEC

of surfactants, could also participate in the different HA adsorption obtained.

The isoelectric points (IEP_{pH}) of OMMT samples, determined as the suspension pH at which the zeta potential attains 0 mV (Tschapek et al. 1989), were 6.5, 4.2, and 5.0 for TDTMA1-MMT, TDTMA2-MMT (from Fig. 6a), and HDTMA2-MMT (from Bianchi et al. 2013), respectively. The positive zeta potential values in all pH ranges studied for HDTMA1-MMT sample (Bianchi et al. 2013) did not allow inferring its IEP_{pH} value by this method.

Also, the decrease of IEP_{pH} values with surfactant loading agrees with the HA adsorbed for TDTMA-MMT but not for HDTMA-MMT samples. The higher positive surface charge of HDTMA1-MMT than TDTMA1-MMT samples could explain the 100 % HA adsorption in a wide HA concentration range. However, higher micelle formation by HDTMA2-MMT than TDTMA2-MMT samples could inhibit HA adsorption despite their similar zeta potential and IEPpH values.

Figure 6b, c show the zeta potential curves for HA alone and those of HA adsorbed on OMMT samples. In Fig. 6b, the negative zeta potential of HA and its shift to more negative values with increasing pH were characteristic of anionic polyelectrolytes with carboxylic functional groups (Zhang and Bai 2003). The HA adsorbed on HDTMA1-MMT and HDTMA2-MMT (Fig. 6b) and TDTMA1-MMT and TDTMA2-MMT (Fig. 6c) samples increased the negative charge value of respective OMMT samples, originated by the expulsion of an acidic hydrogen from the carboxylic acid group of the HA molecule, generating a more negatively charged surface (Anirudhan and Ramachandran 2007).

4 Conclusions

OMMT samples with one and two CEC loadings of $HDTMA^+$ and $TDTMA^+$ showed changes, with respect to the raw MMT, in properties such as specific surface area, particle size, and interlayer spacing values. The FTIR of OMMT revealed the characteristic bands of the surfactant alkyl chains and micelle formations. The zeta potential values of OMMT samples showed a negative surface charge decrease with respect to that obtained for MMT. In both OMMT samples, the excess of each surfactants in respect to the respective CMC values, and arrangements of the adsorbed surfactants generated

a decrease of the zeta potential related to the alkylammonium length chain.

The negative surface charge increase with HA adsorption, within each OMMT samples, was assigned to the negatively charged HA.

The HA adsorption percentage correlated with TSA and negative zeta potential values within each surfactant.

Acknowledgments The authors acknowledge the technical help from G. Guzman and ANPCyT through Project PICT 1360/2006 and FONARSEC FS Nano-008/2010 for financial support of this work. MF acknowledges a fellowship research grant from MINCyT-ANPCyT and CONICET.

References

Anirudhan, T. S., & Ramachandran, M. (2007). Surfactant-modified bentonite as adsorbent for the removal of humic acid from wastewaters. *Applied Clay Science, 35*, 276–281.

Avisar, D., Primor, O., Gozlan, I., & Mamane, H. (2010). Sorption of sulfonamides and tetracyclines to montmorillonite clay. *Water, Air, and Soil Pollution, 29*, 439–450.

Bianchi, A. E., Fernández, M., Pantanetti, M., Viña, R., Torriani, I., Torres Sánchez, R. M., et al. (2013). ODTMA and HDTMA Organomontmorillonites characterization: new insight by WAXS, SAXS and surface charge. *Applied Clay Science, 83–84*, 280–285.

Bojemueller, E., Nennemann, A., & Lagaly, G. (2001). Enhanced pesticide adsorption by thermally modified bentonites. *Applied Clay Science, 18*, 277–284.

Daifullah, A. A., Girgis, B. S., & Gad, H. M. (2004). A study of the factors affecting the removal of humic acid by activated carbon prepared from biomass material. *Colloids and Surfaces A, 235*, 1–10.

Dekov, V. M., Komy, Z., Araújo, F., Van Put, A., & Van Grieken, R. (1997). Chemical composition of sediments, suspended matter, river water and ground water of the Nile (Aswan-Sohag traverse). *Science of the Total Environment, 201*(3), 195–210.

Doulia, D., Leodopoulos, C., Gimouhopoulos, K., & Rigas, F. (2009). Adsorption of humic acid on acid-activated Greek bentonite. *Journal of Colloid and Interface Science, 340*, 131–141.

Fernández, M. A. (2012).Thesis. Utilización de arcillas naturales argentinas y órgano arcillas para la retención de compuestos derivados de la materia orgánica de suelo. Univ. Nac. de Quilmes.

Fernández, M., Cosp, J., Pérez Recuerda, R., Assiego Larriva, M., & Torres Sánchez, R. M. (2011). Caracterización y evaluación de una bentonita argentina, sus productos de tratamientos mecánicos y una española para la potabilización de aguas. In A. M. da Silva, G. Galindo, & J. L. Fernandez Turiel (Eds.), *Aguas, suelos y vegetación en Iberoamérica* (pp. 85–98). Salamanca: Soc. Iberoamericana de Física y Química Ambiental.

Frimmel, F. H., & Christman, R. F. (1988). *Humic substances and their role in the environment*. N York: John Wiley and Sons.

Froehner, S., Fernandes Martins, R., Furukawa, W., & Risso Errera, M. (2009). Water remediation by adsorption of phenol onto hydrophobic modified clay. *Water, Air, and Soil Pollution, 199*, 107–113.

Fuguet, E., Ráfols, E., Martí Rosés, C., & Bosch, E. (2005). Critical micelle concentration of surfactants in aqueous buffered and unbuffered systems. *Analytica Chimica Acta, 548*, 95–100.

Furukawa, K., & Takahashi, Y. (2008). Effect of complexation with humic substances on diffusion of metal ions in water. *Chemosphere, 73*, 1272–1278.

Gieseking, J. E. (1939). The mechanism of cation exchange in the montmorillonite-beidellite-nontronite type of clay minerals. *Soil Science, 47*, 1–13.

Goldani, E., Moro, C. C., & Maia, S. M. (2013). A study employing differents clays for Fe and Mn removal in the treatment of acid mine drainage. *Water, Air, and Soil Pollution, 224*, 1401–1404.

He, H., Frost, R. L., Bostrom, T., Yuan, P., Duong, L., Yang, D., et al. (2006). Changes in the morphology of organoclays with HDTMA surfactant loading. *Applied Clay Science, 31*, 262–271.

He, H., Ma, Y., Zhu, J., Yuan, P., & Qing, Y. (2010). Organoclays prepared from montmorillonites with different cation exchange capacity and surfactant configuration. *Applied Clay Science, 48*, 67–72.

Jiang, J.-Q., Zeng, Z., & Pearce, P. (2004). Preparation and use of modified clay coagulants for wastewater treatment. *Water, Air, and Soil Pollution, 158*, 53–65.

Klepsch, S., Aquino, A. J. A., Haas, U., Tunega, D., Haberhauer, G., Gerzabek, M. H., et al. (2011). Sorption of selected aromatic substances-application of kinetic concepts and quantum mechanical modeling. *Water, Air, and Soil Pollution, 215*(1–4), 449–464.

Lagaly, G., & Weiss, A. (1970). Anordnung und Orientierung kationischer Tenside auf Silicatoberflächen. Teil I. Darstellung der n-Alkylammoniumderivate von glimmerartigen Schichtsilicaten. *Kolloid-Zeitschrift & Zeitschrift für Polymere, 237*, 266–273.

Li, H., Sheng, G., Teppen, B. J., Johnston, C. T., & Boyd, S. A. (2003). Sorption and desorption of pesticides by clay minerals and humic acid-clay complexes. *Soil Science Society of America Journal, 67*(1), 122–131.

Li, Z., Jiang, W.-T., & Hong, H. (2008). An FTIR investigation of hexadecyltrimethyl ammonium intercalation into rectorite. *Spectrochimica Acta Part A, 71*, 1525–1534.

Lombardi, B., Torres Sánchez, R. M., Eloy, P., & Genet, M. (2006). Interaction of thiabendazole and benzimidazole with montmorillonite. *Applied Clay Science, 33*, 59–65.

Magnoli, A. P., Tallone, L., Rosa, C. A. R., Dalcero, A. M., Chiacchiera, S. M., & Torres Sanchez, R. M. (2008). Commercial bentonites as detoxifier of broiler feed contaminated with aflatoxin. *Applied Clay Science, 40*, 63–71.

Michot, L. J., & Villieras, F. (2006). Surfac area and porosity. In F. Bergaya, B. K. Theng, & G. Lagaly (Eds.), *Handbook of clay science* (pp. 965–978). Amsterdam: Elsevier.

Mishael, Y. G., Undabeytia, T., Rytwo, G., Papahadjopoulos-Sternberg, B., Rubin, B., & Nir, S. (2002). Sulfometuron incorporation in cationic micelles adsorbed on

montmorillonite. *Journal of Agricultural and Food Chemistry, 50*, 2856–2863.

Naranjo, P., Sham, E. L., Rodríguez Castellón, E., Torres Sánchez, R. M., & Farfán Torres, E. M. (2013). Identification and quantification of the interaction mechanisms between the cationic surfactant HDTMA-Br and montmorillonite. *Clays and Clay Minerals, 61*(2), 98–106.

Noudeh, G. D., Housaindokht, M., & Fazly Bazzaz, B. S. (2007). The effect of temperature on thermodynamic parameters of micellization of some surfactants. *Applied Clay Science, 7*, 47–52.

Park, Y., Ayoko, G. A., & Frost, R. L. (2011). Characterisation of organoclays and adsorption of p-nitrophenol: environmental application. *Journal of Colloid and Interface Science, 360*, 440–456.

Pospíšil, M., Capková, P., Merínská, Weiss, Z., Maláč, S., & Simoníkz, J. (2002). Intercalation of octadecylamine into montmorillonite: molecular simulations and XRD analysis. *Journal of Colloid and Interface Science, 245*, 126–132.

Praus, P., Turicová, M., Študentová, S., & Ritz, M. (2006). Study of cetyltrimethylammonium and cetylpyridinium adsorption on montmorillonite. *Journal of Colloid and Interface Science, 304*, 29–36.

Radian, A., Carmeli, M., Zadaka-Amir, D., Nir, S., Wakshal, E., & Mishael, Y. G. (2011). Enhanced removal of humic acid from water by micelle-montmorillonite composites: comparison to granulated activated carbon. *Applied Clay Science, 54*, 258–263.

Ruiz-Hitzky, E., Aranda, P., Darder, M., et al. (2010). Hybrid materials based on clays for environmental and biomedical applications. *Journal of Materials Chemistry, 20*, 9306–9321.

Shah, K. J., Mishra, M. K., Shukla, A. D., Imae, T., & Shah, D. O. (2013). Controlling wettability and hydrophobicity of organoclays modified with quaternary ammonium surfactants. *Journal of Colloid and Interface Science, 407*, 493–499.

Stevenson, F. J., & Goh, K. M. (1971). IR spectra of humic acids and related substances. *Geochimia et Cosmochimia Acta, 35*, 471–483.

Theng, B. K., Churchman, G. J., Gates, W. P., & Yuan, G. (2008). Organically modified clays for pollutant uptake and environmental protection. In Q. Huang, P. M. Huang, & A. Violante (Eds.), *Soil mineral-microbe-organic interactions: theories and applications* (pp. 145–174). Berlin: Springer.

Thomas, F., Michot, L. J., Vantelon, D., Montargès, E., Prélot, E. B., Cruchaudet, M., et al. (1999). Layer charge and electrophoretic mobility of smectites. *Colloids and Surfaces, A, 159*, 351–358.

Torres Sánchez, R. M., & Falasca, S. (1997). Specific surface and surface charges of some Argentinian soils. *Zeitschrift für Pflanzenernährung und Bodenkunde, 160*, 223–226.

Tschapek, M., Torres Sánchez, R. M., & Wasowski, C. (1989). Handy methods for determining the isoelectric point of soils. *Zeitschrift für Pflanzenernährung und Bodenkunde, 152*, 73–76.

van Wijk, D., Gyimesi-van den Bos, M., Garttener-Arends, I., Geurts, M., Kamstra, J., & Thomas, P. (2009). Bioavailability and detoxification of cationics: I. Algal toxicity of alkyltrimethyl ammonium salts in the presence of suspended sediment and humic acid. *Chemosphere, 75*, 303–309.

Vermeer, W. P., van Riemsdijk, W. H., & Koopal, L. K. (1998). Adsorption of humic acid to mineral particles. 1. Specific and electrostatic interactions. *Langmuir, 14*, 2810–2819.

White, G. C. (1999). *Handbook of chlorination and alternative disinfectants, chap. 12*. New York: Wiley-Interscience Publication.

Zadaka, D., Radian, A., & Mishael, Y. G. (2010). Applying zeta potential measurements to characterize the adsorption on montmorillonite of inorganic, cations as monomers, micelles or polymers. *Journal of Colloid and Interface Science, 352*, 171–177.

Zhan, Y., Zhu, Z., Lin, J., Qiu, Y., & Zhao, J. (2010). Removal of humic acid from aqueous solution by cetylpyridinum bromide modified zeolite. *Journal of Environmental Science, 22*(9), 1327–1334.

Zhang, X., & Bai, R. (2003). Mechanisms and kinetics of humic acid adsorption onto chitosan-coated granules. *Journal of Colloid and Interface Science, 264*, 30–38.

Zhu, J., He, H., Guo, J., Yang, D., & Xie, X. (2003). Arrangement models of alkylammonium cations in the interlayer of HDTMA+ pillared montmorillonites. *Chinese Science Bulletin, 48*, 368–372.

Zhu, J., He, H., Zhu, L., Wen, X., & Deng, F. (2005). Characterization of organic phases in the interlayer of montmorillonite using FTIR and 13C NMR. *Journal of Colloid and Interface Science, 286*, 239–244.